

Time-dependent contrast functions for quantitative imaging in time-resolved transillumination experiments

Amir H. Gandjbakhche, Victor Chernomordik, Jeremy C. Hebden, and Ralph Nossal

We have developed a methodology that can be used in reconstruction algorithms to quantify the optical coefficients and the geometrical cross section of a weakly abnormal optical target embedded in an otherwise homogeneous medium. This novel procedure uses different time-dependent point-spread functions to analyze the diffusive and absorptive contrasts obtained from time-of-flight measurements. Data obtained from time-resolved transillumination of a tissuelike phantom are used to test the accuracy of this new deconvolution methodology.

OCIS code: 100.1830.

1. Introduction

Optical imaging has attracted significant interest as a potential noninvasive diagnostic tool for detecting tumors and other abnormalities hidden in thick biological tissues.¹⁻⁴ For this purpose various techniques such as frequency-resolved, time-resolved, and cw techniques that use different geometries (e.g., transillumination) have been proposed. Until now, most image-reconstruction schemes have been devised for the frequency-domain technique in which one uses the measured phase and intensity to quantify the position, the optical properties, and the geometric cross section of the abnormal target(s). When these reconstruction techniques are applied to real experiments, in which realistic values of differences between the optical characteristics of the abnormal target and normal background (e.g., those reported in 5) are used, the location of the centroid of the abnormal target is easily found. However, quantification of the optical properties of the target with reasonable resolution (i.e., reconstruction of the cross section) still remains a challenging task.⁶⁻⁸

In the present paper we focus on time-resolved

transillumination. Because conventional transillumination results in poor resolution of abnormal regions, improvement of spatial resolution is required and can be obtained, in principle, by the time-gated detection of photons.⁹ Unfortunately, the low level of detected intensity of those photons that reach the detector at early times (e.g., quasi-ballistic photons) makes high spatial resolution of the target clinically difficult.^{10,11} Thus, for example, for a 55-mm-thick breast-tissuelike phantom it has been found that an adequate level of light is detected only after a time of 500 ps in excess of the true ballistic transit of 220 ps.¹² However, even though for these longer delay times an image is degraded by the long trajectories of the detected photons, the presence of an abnormal site (which has optical properties that differ from those of the background normal tissue) still perturbs photon paths inside the tissue. Here we propose a new methodology based on time-dependent contrast functions to discriminate between the absorptive and the diffusive perturbations caused by an abnormal target. Moreover, to substantiate our methodology, instead of using simulated data or unrealistic characteristics of the abnormal target we used time-of-flight experiments performed on a challenging phantom whose thickness and optical properties, and the characteristics (size and optical properties) of the abnormal target, mimic a human breast. To our knowledge, this use of time-dependent contrast functions is novel.

The simplest descriptions of photon trajectories inside a turbid medium that contains an embedded abnormality utilize diffusionlike models such as the

A. H. Gandjbakhche, V. Chernomordik, and R. Nossal are with the Laboratory of Integrative and Medical Biophysics, National Institute of Child Health and Human Development, National Institutes of Health, Bethesda, Maryland 20892. J. C. Hebden is with the Department of Medical Physics, University College, London WC1E 6JA, UK.

Received 30 June 1997; revised manuscript received 4 November 1997.

diffusion approximation of transport theory^{13,14} or a lattice random-walk model.¹⁵ Even in those models, expressions for perturbation kernels may still be quite complicated, making the fitting or the iteration of experimental data quite difficult unless adequate approximations can be found. We previously derived the time-dependent contrast functions associated with an abnormally absorbing region.¹⁵ Using the same methodology, here we determine the contrast functions for a weak scattering abnormality embedded in an otherwise optically homogeneous medium. By combining these contrast functions we now devise a methodology, used in an inverse algorithm, that enables us to reconstruct the optical properties and the cross section of a region in which the scattering and the absorption are both abnormal. This algorithm makes use of a recently found Gaussian approximation to the point-spread function.^{11,16}

In Section 2 we describe the theoretical model and compare the diffusive and the absorptive contrasts with those obtained from more-rigorous derivations based on the diffusion approximation to the transport equation.¹³ In Section 3 we apply our model to a set of measurements that were performed on a tissuelike phantom at University College London. In Section 4 we comment on the significance of our research and also on the limitations and the pertinence of the approximations made in our analysis.

2. Theoretical Model

The theoretical development presented here is based on the theory of lattice random walks in which the tissue continuum is replaced by a simple cubic lattice and photons are represented by random walkers permitted to move only between lattice points.¹⁷ In this picture scattering events are replaced by steps taken by a random walker moving from one lattice site to another. The tissue structure is considered to be homogeneous, except for a compact region containing an abnormal site at which the scattering and the absorption coefficients are both different from those of the background. The tissue is modeled as an infinite slab, N lattice units thick, separated from the exterior by two planes at $z = 0$ and $z = N$. Points in the interior of the tissue are represented by $z > 0$, whereas values of x and y can assume all integer values from $-\infty$ to ∞ , which are then converted into dimensioned units.

In our model a single photon is introduced into the medium at time step zero, at point $\mathbf{r}_0 = (0, 0, 1)$. The photon exits the medium at step n and is detected at point $\mathbf{r} = (x, y, N)$. An abnormal mass is assumed to be located at $\mathbf{s} = (s_1, s_2, s_3)$. This abnormal site is assumed to have two properties that differ from those of the other lattice sites. First, when a photon reaches \mathbf{s} it can be absorbed with some excess probability $\eta < 1$ compared with its activity with other sites where the probability is μ (with $\mu \ll 1$). Second, the photon experiences some additional steps or time delay, Δn_D , while it is moving across the slab (i.e., in the transmission mode), which is related to an increase in scattering coefficient at the site. In a

description below of the transformation of random-walk parameters into physical variables we relate η , μ , and the average value $\langle \Delta n_D \rangle$ to the actual optical coefficients [see Eqs. (4) below].

The events that lead to the arrival of a photon at the surface can be decomposed into three groups, with associated times n_1 , Δn_D , and n_3 :

1. First, the photon moves from the source to site \mathbf{s} . It then may recirculate, leaving site \mathbf{s} and returning an arbitrary number of times. This first group of events takes n_1 steps.
2. The photon is delayed for Δn_D steps because of the increased scattering cross section of \mathbf{s} .
3. The photon finally leaves \mathbf{s} and moves in n_3 steps to a point one lattice unit below the surface from which, one step later, it exits the material. Exit time n thus satisfies the relation $n_1 + \Delta n_D + n_3 = n - 1$.

Let $p_n(\mathbf{r}|\mathbf{r}_0)$ and $q_n(\mathbf{s}, \mathbf{r}|\mathbf{r}_0)$ be, respectively, the probabilities that a photon injected at \mathbf{r}_0 at $n = 0$ is at $\mathbf{r} = (x, y, N)$ at step n , without and with the presence of an abnormal site at \mathbf{s} in the slab. One can define the contrast, $C(\mathbf{s}, \mathbf{r}|\mathbf{r}_0, n)$, to be

$$C(\mathbf{s}, \mathbf{r}|\mathbf{r}_0, n) = \frac{p_n(\mathbf{r}|\mathbf{r}_0) - q_n(\mathbf{s}, \mathbf{r}|\mathbf{r}_0)}{p_n(\mathbf{r}|\mathbf{r}_0)} = 1 - \frac{q_n(\mathbf{s}, \mathbf{r}|\mathbf{r}_0)}{p_n(\mathbf{r}|\mathbf{r}_0)}, \quad (1)$$

from which we define the quantity $I(\mathbf{s}, \mathbf{r}|\mathbf{r}_0, n) = p_n(\mathbf{r}|\mathbf{r}_0) - q_n(\mathbf{s}, \mathbf{r}|\mathbf{r}_0)$ to be the perturbation amplitude.

Previously it was shown that, for small values of η (i.e., $\eta \ll 1$) the absorptive contrast can be expressed as¹²

$$C_A(\mathbf{r}|\mathbf{r}_0, n) = \eta \frac{W(\mathbf{s}, \mathbf{r}, \mathbf{r}_0)_{n+1}}{p_n(\mathbf{r}|\mathbf{r}_0)}, \quad (2)$$

where $W(\mathbf{s}, \mathbf{r}, \mathbf{r}_0)_n$ is the probability that the photon, after entering the material at \mathbf{r}_0 , visits \mathbf{s} and is detected at \mathbf{r} at the n th step. Using the same methodology as is presented in Ref. 15, we have derived an expression for the contrast that arises from a slight increase in the scattering properties of \mathbf{s} above those of the background. The effect of such scattering aberration is modeled by an increase in the number of steps in the random walk of the photon, leading, as shown in Appendix A, to the following expression for the diffusive contrast:

$$C_D(\mathbf{s}, \mathbf{r}|\mathbf{r}_0, n) = \frac{W(\mathbf{s}, \mathbf{r}, \mathbf{r}_0)_n - W(\mathbf{s}, \mathbf{r}, \mathbf{r}_0)_{n-1}}{p_n(\mathbf{r}|\mathbf{r}_0)} \langle \Delta n_D \rangle. \quad (3)$$

Although derivations of the absorptive and the diffusive contrasts given by Eqs. (2) and (3) were done separately, the assumptions of both derivations are the same. In both instances we suppose that perturbations in photon paths induced by the inclusion are small (i.e., that $\eta \ll 1$ and $\langle \Delta n_D \rangle \ll n$), which

allows us to use the product of two Green's functions, $\hat{p}_\xi(\mathbf{s}|\mathbf{r}_0)$ and $\hat{p}_\xi(\mathbf{r}|\mathbf{s})$ (see Appendix A).

The numerator of Eq. (3) is the discrete equivalent of the derivative of the point-spread function at \mathbf{s} . Hence the largest contribution of scattering perturbations to the overall contrast is expected for small values of n , where the slope of W_n as a function of n is steepest. The influence of scattering perturbations that is due to the inclusion becomes less and less significant when n is large. Later in this section we explicitly describe the function W_n and its Gaussian counterpart [Eqs. (7) and (8)].

Now let us relate the dimensionless variables of the lattice random walk to actual physical variables¹⁵:

$$\begin{aligned} \mu &\rightarrow \frac{\mu_a}{\mu_s'}, & n &\rightarrow \mu_s' ct, & \mathbf{r} &\rightarrow \frac{\bar{\mathbf{r}}\mu_s'}{\sqrt{2}}, \\ N &\rightarrow \frac{T'\mu_s'}{\sqrt{2}}, & \eta &\rightarrow \frac{\tilde{\mu}_a - \mu_a}{\mu_s'}, \end{aligned} \quad (4)$$

where μ_a and μ_s' are the absorption- and the transport-corrected scattering coefficients of the background in inverse millimeters, c is the speed of light in the medium in millimeters per picosecond, t is the time in picoseconds, T and $\bar{\mathbf{r}}$ are the thickness of the slab and the distance variable, respectively, in millimeters, and $T' = T + \sqrt{2}/\mu_s'$. The absorption coefficient of the abnormal inclusion is $\tilde{\mu}_a$.

In diffusionlike processes, which are probabilistic in nature, the pertinent variables are the mean-square displacement and the number of steps or time. Thus one can relate the quantity $\langle \Delta n_D \rangle$ to the scattering coefficient $\tilde{\mu}_s'$ and the size d of the inclusion by using the relation between the mean-square displacement $\langle l^2 \rangle$ and the number of steps m of an isotropic random walk. For exponentially distributed scattering lengths the latter is given as $\langle l^2 \rangle \approx 2m$,¹⁸ which, in terms of actual variables, takes the form $\tilde{\mu}_s'^2 \langle d_1^2 \rangle = 2c\tau_1\tilde{\mu}_s'$, where $\tau_1 = m/(c\tilde{\mu}_s')$ is the time spent by photons to achieve a mean-square displacement $\langle d_1^2 \rangle$ inside the inclusion. Similarly, when the photon migrates within the normal scattering medium, say, for a time τ_2 , the corresponding mean-square displacement is $\mu_s'^2 \langle d_2^2 \rangle = 2c\tau_2\mu_s'$. Thus, for an equal mean-square displacement $\langle d_1^2 \rangle = \langle d_2^2 \rangle = \langle d^2 \rangle$, the extra time $\Delta\tau = \tau_1 - \tau_2$ taken by the photon to migrate a given distance $\langle d^2 \rangle$ owing to increased scattering is

$$\Delta\tau = \tau_1 - \tau_2 = \frac{\langle d^2 \rangle (\tilde{\mu}_s' - \mu_s')}{2c}, \quad (5)$$

which, in terms of random-walk variables, is

$$\langle \Delta n_D \rangle = c\mu_s' \Delta\tau = \frac{\langle d^2 \rangle \mu_s' (\tilde{\mu}_s' - \mu_s')}{2}. \quad (6)$$

Because photons will spend more time at an abnormal site when an inclusion has increased scattering, η in Eq. (1) has to be replaced by $\eta_{\text{eff}} = K\eta$, where K is defined as $K = \tilde{\mu}_s'/\mu_s'$. In the treatment that

follows, we consider that the inclusion might extend over several contiguous lattice sites, in which case the resulting absorptive and diffusive contrasts are considered the sum of the individual contributions of each abnormal site. This approximation is valid for small perturbations and target size (compared with the dimensions of the slab).

The exact expression for $W(\mathbf{s}, \mathbf{r}, \mathbf{r}_0)_n$ in the special case $\mathbf{r} = (x, 0, N)$, $\mathbf{r}_0 = (0, 0, 1)$, is^{11,15,16}

$$\begin{aligned} W(\mathbf{s}, \mathbf{r}, \mathbf{r}_0)_n &= \frac{9}{16\pi^{5/2}(\Delta n)^{3/2}} \\ &\times \sum_{k=-\infty}^{\infty} \sum_{m=-\infty}^{\infty} \{F_n[\alpha_-(k), \beta_-(m, x)] \\ &+ F_n[\alpha_+(k), \beta_+(m, x)] \\ &- F_n[\alpha_+(k), \beta_-(m, x)] \\ &- F_n[\alpha_-(k), \beta_+(m, x)]\}, \end{aligned} \quad (7)$$

where

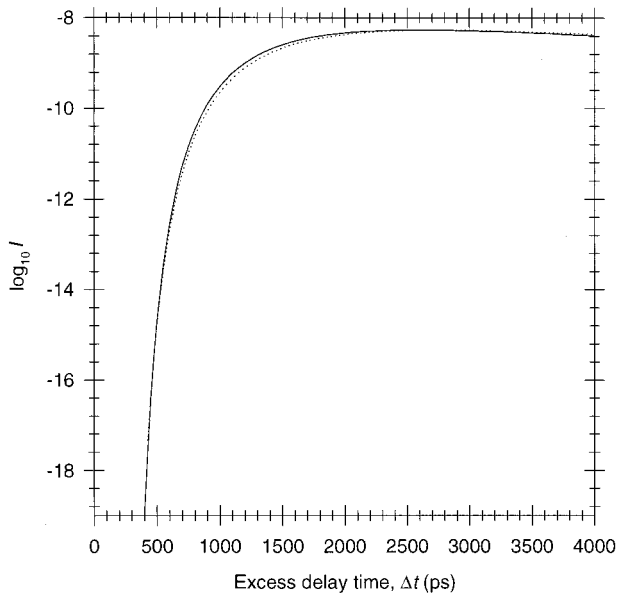
$$\begin{aligned} \Delta n &= \mu_s' c \Delta t, \\ F_n(a, b) &= \left(\frac{1}{a} + \frac{1}{b} \right) \exp \left[- \frac{(a+b)^2}{\Delta n} \right], \\ \alpha_{\pm}(k) &= \{ \frac{3}{2} [s_1^2 + (s_3 + 2kN \pm 1)^2] \}^{1/2}, \\ \beta_{\pm}(m, x) &= \{ \frac{3}{2} [(x - s_1)^2 + (N - s_3 + 2mN \pm 1)^2] \}^{1/2}. \end{aligned} \quad (8)$$

[We have assumed that $s_2 = 0$, i.e., $\mathbf{s} = (s_1, 0, s_3)$, which corresponds to line-scan measurements.] Previously we showed that this complicated expression can be approximated with a simple Gaussian distribution that can be characterized in terms of its standard deviation σ . For transillumination, σ is given, in real variables, as^{11,16}

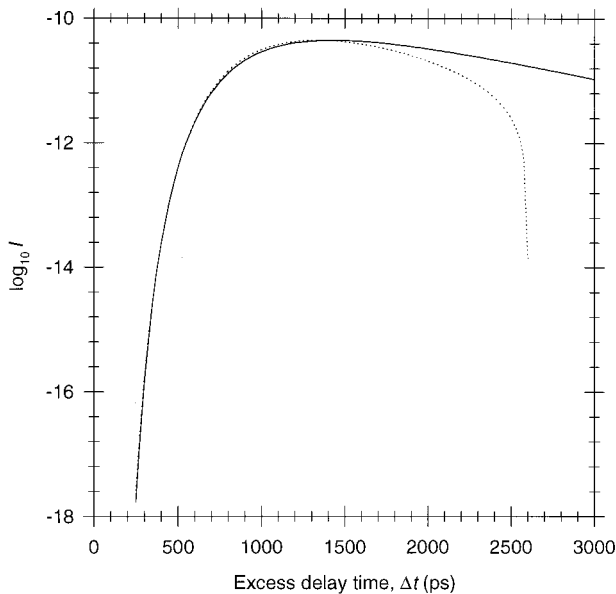
$$\sigma = 0.816 \left(\frac{c\Delta t}{\mu_s'} \right)^{1/2} \left[\left(1 - \frac{\bar{s}_3}{T'} \right) \frac{\bar{s}_3}{T'} \right]^{1/2}, \quad (8)$$

where Δt is the excess transit time of the imaging system and \bar{s}_3 is the depth of the inclusion in physical units. Note that the maximum value of σ is obtained at the midplane ($\bar{s}_3 = T'/2$). Equation (8) is used in the data fitting described in Section 3.

Before further analysis, let us compare our simple expressions for the absorptive perturbation and diffusive perturbation amplitudes [numerators of Eqs. (2) and (3)] with those obtained by Arridge,¹³ who used a standard perturbation theory of the diffusion approximation to the transport equation. Parameters chosen here, for illustration, are close to those of the phantom analyzed in Section 3: $\mu_s' \approx 0.7 \text{ mm}^{-1}$, $T = 55 \text{ mm}$, and $n_r \approx 1.56$ [where n_r is the refractive index that one needs to calculate c ; see Eqs. (4)–(6)]. The source, the target (at midslab), and the detector are taken to be collinear. In Fig. 1, perturbation amplitudes of our model (dotted curves) are compared with those of Arridge (solid curves). The absorptive perturbation amplitudes [Fig. (1a)] and early-time behavior of the diffusive perturbation amplitudes



(a)



(b)

Fig. 1. Comparison between (a) absorptive and (b) scattering perturbations [Eq. (1) ff.] of the diffusion model of Arridge⁸ (solid curves) and the random-walk model (dotted curves) as a function of the gating time Δt for a detector collinear with the source and point s .

[Fig. (1b); up to their maxima] for the two models are in excellent agreement. However, the asymptotic behavior of the diffusive perturbation calculated from the Arridge model tends to zero more slowly (data not shown) than in our case (see approximations discussed in Appendix A and Section 4).

The basic assumption of our approach is to separate the contribution of diffusive and absorptive perturbations; that is, our analysis makes use of the different dependences of the contrasts on time delay Δt of the transillumination imaging system, as illustrated in Fig. 2. The sum of the two contrasts is also

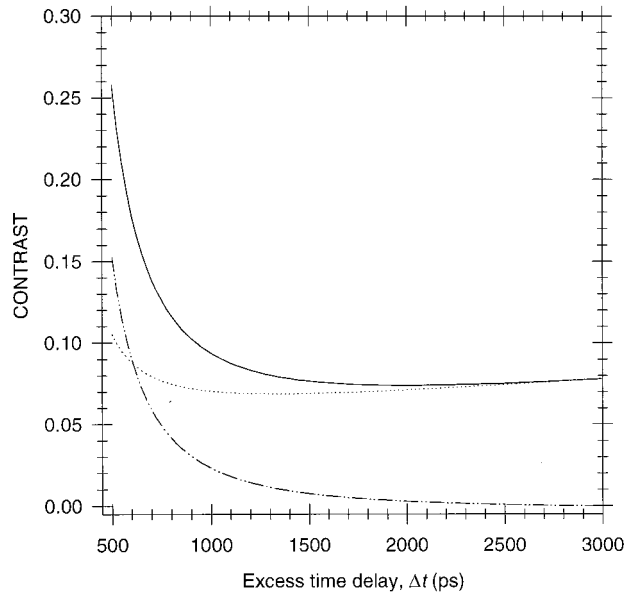


Fig. 2. Behavior of absorbing (dotted curve) and scattering (dash-dotted curve) contrasts and their sum (solid curve) as a function of the gating time Δt . At short Δt the scattering perturbation is dominant, whereas at large Δt the total contrast is exclusively dependent on the absorptive perturbation.

shown. (These theoretical calculations are done for a slab 55 mm thick that has optical coefficients of $\mu_a = 0.0056 \text{ mm}^{-1}$ and $\mu_s' = 0.77 \text{ mm}^{-1}$ and contains an embedded cubic target of size $d = 5 \text{ mm}$ on a side whose scattering and absorption coefficients are twice those of the surrounding medium; although these parameters are close to those of the experimental phantom on which our data analysis is performed, any reasonable set of parameters could have been used.) It can easily be seen from this figure that for relatively large Δt ($\Delta t > 1500 \text{ ps}$) the main contribution to the total contrast, which is nearly independent of Δt , is due to the absorptive component. In comparison, for small time delays ($\Delta t < 700 \text{ ps}$), contrast amplitude rises steeply with decreasing Δt because of an increasing contribution of the diffusive, scattering contrast component. As has been shown in Ref. 15 (and can be seen from Fig. 2), the absorptive component also increases with decreasing Δt but at considerably smaller values of Δt , and its relative change is smaller than that of the diffusive component. Hence, as we show in Section 3, one can use the short Δt range to estimate the magnitude of the diffusive perturbation if η_{eff} and the corresponding absorptive contrast component are first determined from experimental data that pertain to large Δt .

3. Data Analysis

To illustrate our approach we used streak-camera data provided by investigators working at University College London. These researchers studied a phantom made from a single perturbing cylinder, of diameter 5 mm and length 5 mm, located midway between the two faces of a rectangular slab of thickness $T = 55$

mm. Measurements were made in the so-called fan geometry, in which the beam from a point laser source is aligned exactly with the center of the target and the detector is moved (in 1-mm steps; total 51 steps) along a single line (x axis) on the opposite side of the slab. Temporal path-length distributions $I(x, \Delta t)$ were experimentally obtained for each position of the detector. However, because of low intensity, no photon data were provided for $\Delta t < 500$ ps.

Our goal was to determine the optical properties of the background and those of the inclusion, along with its size, from existing data. To perform our reconstruction we made use of the knowledge that the inclusion is located at the middle of the slab. (Off-axis scans of the source, and analysis of the resulting two-dimensional images, are required for the depth of the target to be determined.) We first fitted all the experimental $\{I(x, \Delta t)\}$ to theoretical path-length distributions for a homogeneous slab.¹⁹ To do so we took account of an evident geometrical modification for the lateral shift of the source and the detector, which, in the case of the fan geometry and in the framework of the random-walk model, is an additional exponential factor to those in the transillumination case (source and detector colinear), viz.,¹⁹

$$I^{(f)}(x, \Delta t) \equiv I^{(t)}(\Delta t) \exp(-3\mu_s' x^2 / 4c\Delta t). \quad (9)$$

The fitting parameters are the scattering and absorption coefficients (μ_s' , μ_a), the amplitude constant of $I(x, \Delta t)$, and an adjustable time shift δt relative to the nominal time that the photons enter the material. For each detector position we determined the maximal value of the fitted intensities. This quantity changes as the detector is moved with respect to the source. The path-length distribution corresponding to the highest value, $I_0(\Delta t)$, was assumed to be the unperturbed path-length distribution, and we used it to determine values of the scattering and absorption coefficients inside the slab. The experimental curve and the theoretical fit are presented in Fig. 3. From the fit we obtained the values $\mu_s' \approx 0.77 \text{ mm}^{-1}$ and $\mu_a \approx 0.0056 \text{ mm}^{-1}$, which agree well (within $\sim 10\%$) with the optical parameters of the phantom, for which the predetermined values were refractive index $n_r \approx 1.56$, $\mu_s' \approx 0.7 \text{ mm}^{-1}$, and $\mu_a \approx 0.006 \text{ mm}^{-1}$.

Then, for a chosen set of time delays $\Delta t = 750, 800, 900, 1000, 1200, 1500, 2000, 2500, 3000$ ps, intensity contrasts $C(x, \Delta t)$ were calculated for different values of scan position x (i.e., detector positions). In the case of scanning with a coaxial source and detector (so-called transillumination geometry), one can use the simple formula $C(x, \Delta t) \equiv [I_0(\Delta t) - I(x, \Delta t)] / I_0(\Delta t)$ to estimate contrast. However, in the case of fan geometry one requires corrections similar to those that lead to Eq. (9) to obtain corresponding transil-

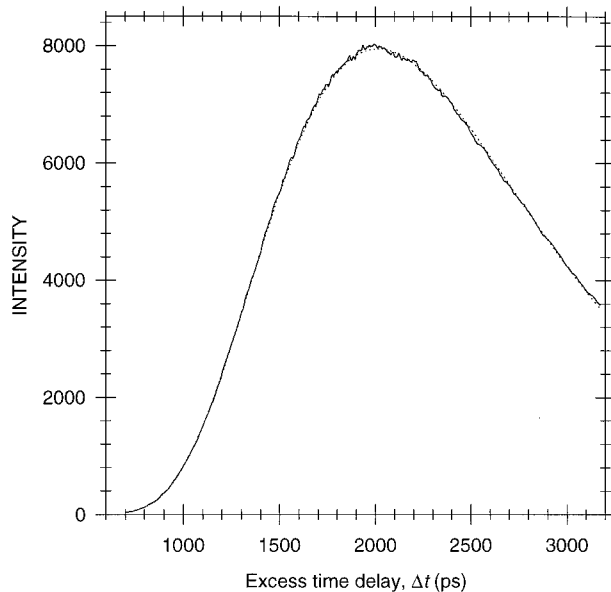


Fig. 3. Time-of-flight curve of maximum intensity obtained in the line-scan measurement (solid curve; see text). The dotted curve is the theoretical fit, from which the optical properties of the background are calculated.

lumination contrasts, $C_T(x, \Delta t)$, from the raw experimental data (see Appendix B); viz.,

$$C_T(x, \Delta t) = \left[1 - \frac{I^{(f)}(x, \Delta t) p_{\Delta t}(x_0)}{I_0^{(f)}(x_0, \Delta t) p_{\Delta t}(x)} \right] \times \frac{W^{(t)}(\mathbf{s}, \mathbf{x})_{\Delta t} p_{\Delta t}(x)}{W^{(f)}(\mathbf{s}, \mathbf{x})_{\Delta t} p_{\Delta t}(0)}, \quad (10)$$

where indices t and f in $W(\mathbf{s}, \mathbf{x})_n$ correspond, respectively, to the transillumination and the fan geometries and x_0 is the position of the detector for the unperturbed path-length distribution [see Eq. (9) ff.].

Experimental contrast functions were then fitted to the theoretical contrasts given by Eqs. (2) and (3). For the sake of simplicity the inclusion was represented by N_a^3 independent, identical target lattice points forming a cube of $N_a \times N_a \times N_a$ elements. N_a is an input parameter. The fitting parameters are the effective absorptivity of an elementary absorber η_{eff} , a scale factor for the contrast $A_{\Delta C}$ determined by a least-squares fit to the data, the position of the center of the inclusion x_i , and the inferred effective distance d_s between neighboring lattice sites in the target. Theoretically, parameter d_s should have a value close to that of the lattice spacing of the background, i.e., $d_s \approx \sqrt{2}/\mu_s'$. Although d_s varies with the choice of the number of presumed target lattice points N_a , one criterion for deciding the proper value of N_a is to see how close the computed value of d_s is to the inferred lattice spacing of the background (1.83 mm for the phantom). The product $d = (N_a - 1)d_s$, which varies only weakly with N_a , corresponds to the actual geometric cross section of the target.

To determine the optimal choice of N_a we first fitted

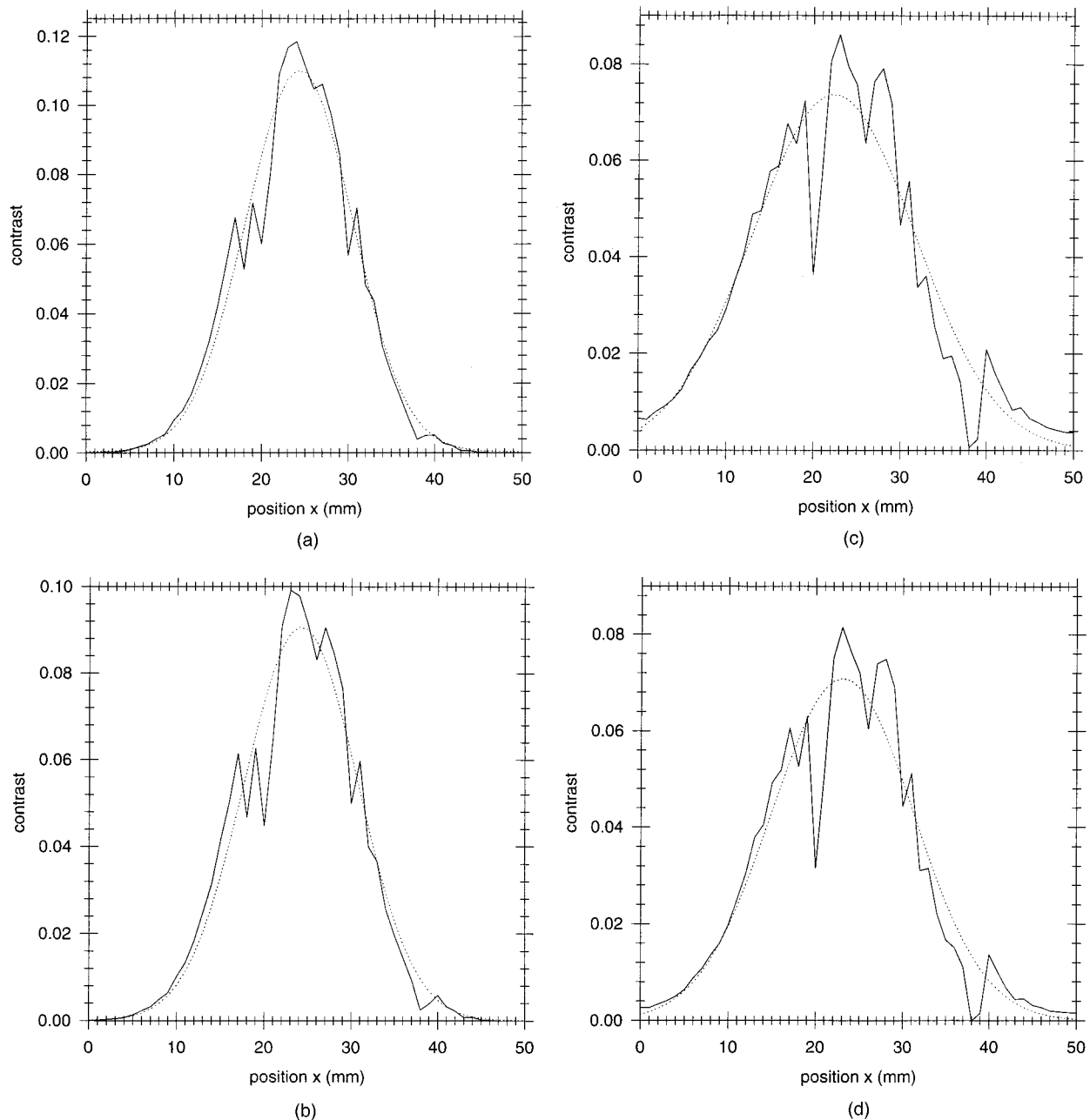


Fig. 4. Experimental total contrast (solid curves) as a function of position x (fan geometry) at $\Delta t =$ (a) 800, (b) 900, (c) 1500, and (d) 2500 ps for $N_\alpha = 4$. The dotted curves are the theoretical fits to the data from Eq. (1). Values of fitting parameters are presented in Section 3. Systematic data fitting to contrast functions for a set of Δt enables one to obtain both the optical coefficients and an estimate for the size of the inclusion (see text).

the measured contrast functions $C_T(x, \Delta t)$ for $\Delta t = 800$ ps for $N_\alpha = 3, 4, 5, 6, 7$. The corresponding values of d_s are 2.5, 1.8, 1.5, 1.2, and 1 mm. Thus the computed values for d are 5, 5.4, 6, 6, and 6 mm. As the closest value of d_s to the actual lattice spacing is that obtained for $N_\alpha = 4$, it was chosen for subsequent calculations of the optical properties. We found that the results mentioned above were invariant with the choice of Δt as long as Δt was less than the value corresponding to the maximal values of the time-resolved intensities.

Using the methodology described above, we then

fitted the contrast functions for different time delays. Some examples of fitted contrasts for $\Delta t = 800, 900, 1500, 2500$ ps are given in Fig. 4. As expected, the observed contrast amplitude decreases considerably in the range $\Delta t = 800$ – 1500 ps, and it is almost constant for longer time delays (Section 2). For $\Delta t = 800$ ps the fit yields $A_{\Delta C} = 0.026$, $x_i = 24.4$ mm, and $d_s = 1.8$ mm. We know that for short time delays the amplitude reflects the contributions of both the absorptive and the diffusive perturbations. Thus we used the amplitude of the fitted contrast for $\Delta t = 2500$ ps (for which the contribution of the dif-

fusive perturbation is negligible) to determine the value $\eta_{\text{eff}} = 0.015$. Once this value was known, we computed $C_A(x, 800)$ from Eq. (2) and subtracted the results from the fitted value of $C(x, 800)$ to obtain $C_D(x, 800)$. The next step involved fitting the latter value by Eqs. (3), (5), and (6) to obtain the values $\langle \Delta n_D \rangle = 9$ and $\Delta \tau = 61$ ps. The absorption and the scattering coefficients of the inclusion were calculated from knowledge of the values of η_{eff} and $\Delta \tau$. From this analysis we found that $\tilde{\mu}_s' = 1.6$ mm and $\tilde{\mu}_a = 0.011$ mm⁻¹, which compare favorably with the known values 1.4 and 0.012 mm⁻¹.

Hence by this method we are able to quantify the optical properties of the target rather well. Further, although there seems to be a difference of approximately 50% between the actual and the computed geometrical cross sections of the target, this discrepancy may be due to several factors that can be minimized, including noise in the data, possible distortion of the target during preparation of the sample, and limited measurements (there being no oblique-angle and off-center source–detector measurements in the supplied data set). Indeed, this figure of 50% may originate in large part from the fact that the present data-acquisition scheme and algorithm implementation cannot distinguish between square and circular cross section; this difference, by itself, is approximately 30%. Significantly, the calculated target dimension d seems to converge as N_a increases ($d = 6.0$ for $N_a = 5, 6, 7$), indicating that little improvement would accrue if one were to subdivide the target onto an increasingly finer mesh when fitting data by algorithms similar to that which is used here.

4. Summary and Discussion

We have devised a new methodology that uses available time-of-flight measurements to deduce the cross section and the optical properties of an abnormality embedded in a homogeneous, optically turbid medium. The novelty of this approach is that it is based on theoretical expressions of absorbing and diffusive contrast functions that have different time-dependent behaviors, allowing one to discriminate between absorbing and scattering contributions to the total detected contrast. Although this method cannot be used for cw measurement because of the approximations used in the analysis (see Appendix A), it compares well with reconstruction methods based on the Born approximation applied to the time-dependent diffusion approximation to the transport equation. A particular strength of our analysis is that it represents the photon point-spread function (which appears in the expressions for the contrasts) by a Gaussian approximation, making the implementation of an inverse method much easier than when complete expressions for the perturbation amplitudes are used.

We applied our method to time-of-flight measurements of a tissuelike phantom and found reasonable values for the overall size and optical properties of an abnormality. In contrast to reconstruction schemes

that employ simulated data for their validation, ours uses real experimental data containing real noise, obtained from a phantom that had finite boundaries. In its present version the algorithm cannot reconstruct the detailed shape of the target, so one obtains an equivalent cubic volume. For the particular phantom explored here, which was chosen because of its similarity to tissue, the discrepancy between estimated and nominal target dimension is approximately 8%, although corresponding variations of the cross section and volume of the inclusion are larger (respectively 50% and 60%). One has to note that only line-scan measurements were available. Moreover, unlike in simulation experiments, the range of Δt over which the measurements were performed corresponds to the diffusive regime of light propagation within the tissue, in which no ballistic or short-path photons are detected.

So far our method has been applied to only one set of measurements, all obtained from the same phantom. This phantom contains an embedded target whose radius is 1/11 of a 55-mm slab thickness. The optical properties of the slab and those of the abnormal target are in the range reported in the literature for real tissue. No other method has provided reasonably accurate, quantitative characterizations of such a realistic phantom. For purposes of simple illustration we used a phantom whose inclusion was known to be in the center of the slab, but straightforward generalization (albeit with much more extensive measurement and calculation, involving oblique-angle source–detector geometry) would allow one to determine the depth of the inclusion as well. However, note that we have quantified the characteristics of a target in the middle of a slab, where the resolution is worst.

We expect to test further the robustness of our method by using a variety of phantoms with different optical properties and thicknesses, and we are refining our inverse algorithm to take into account the edge effects of a finite slab on photon path lengths. Although the algorithm currently presupposes a single abnormal mass located within a homogeneous background, it can readily be generalized to detect and characterize multiple targets. However, issues of detectability, when the target lies within an optically heterogeneous background that is characteristic of real tissue, yet need to be investigated. Finally, we note that no computational scheme will accurately locate and characterize a hidden target if the intrinsic contrast between target and background is low. No scheme will resolve multiple targets that are close together, particularly when their optical properties are close to those of the background.

Appendix A: Derivation of Diffusive Perturbation

As previously,¹⁵ the perturbation induced by the presence of the abnormal target embedded in otherwise homogeneous turbid background can be expressed in terms of the generating functions of the sequences involved in the migration of photons inside the medium.

The generating function for a sequence $\{h_n\}$, which can be regarded as a discrete analog of a Laplace transform, is defined as

$$\hat{h}_\xi = \sum_{n=0}^{\infty} h_n \exp(-\xi n), \quad (\text{A1})$$

in which ξ is the transform variable. For example, let $\psi_{\Delta n_D}$ be the probability distribution in the time domain that a photon is delayed for Δn_D steps while it is at the abnormal site, in which case ψ_ξ is its transform. Similarly, $\hat{p}_\xi(\mathbf{r}|\mathbf{s})$ is the generating function of the probability distribution $p_n(\mathbf{r}|\mathbf{s})$, which is the probability that a photon starting at \mathbf{s} will be found at point \mathbf{r} exactly n steps later.

By following the derivation given in Ref. 15 one finds that a general expression for the perturbation amplitude [see Eq. (1) ff.] can be expressed as

$$\hat{Q}_\xi = \frac{(1 - \hat{\psi}_\xi) \hat{p}_\xi(\mathbf{s}|\mathbf{r}_0) \hat{p}_\xi(\mathbf{r}|\mathbf{s})}{\hat{\psi}_\xi + (1 - \hat{\psi}_\xi) \hat{p}_\xi(\mathbf{s}|\mathbf{s})}. \quad (\text{A2})$$

One has to choose the appropriate model for a given perturbation. In the case of diffusive perturbation, we model the excess delay time at the abnormal site by the geometric distribution $\psi_{\Delta n_D} = (1 - \theta)\theta^{\Delta n_D - 1}$, $\theta \leq 1$, $\Delta n_D = 1, 2, 3, \dots$, where θ is a number between 0 and 1. The average duration of this distribution in discrete time units is $\langle \Delta n_D \rangle = (1 - \theta)^{-1}$, and its generating function is $\hat{\psi}_\xi = (1 - \theta)/(e^\xi - \theta)$. For small ξ one can expand $e^\xi \approx 1 + \xi$ and assume that $\hat{p}_\xi(\mathbf{s}|\mathbf{s}) = 1$ [$\hat{p}_\xi(\mathbf{s}|\mathbf{s})$ is the recirculation probability through \mathbf{s}]. Hence, the perturbation amplitude becomes

$$\hat{Q}_\xi = \langle \Delta n_D \rangle \xi \hat{p}_\xi(\mathbf{s}|\mathbf{r}_0) \hat{p}_\xi(\mathbf{r}|\mathbf{s}). \quad (\text{A3})$$

The inverse transform of $[\xi \hat{p}_\xi(\mathbf{s}|\mathbf{r}_0), \hat{p}_\xi(\mathbf{r}|\mathbf{s})]$ is simply the derivative of W_n with respect to n , viz., $W(\mathbf{s}, \mathbf{r}, \mathbf{r}_0)_n - W(\mathbf{s}, \mathbf{r}, \mathbf{r}_0)_{n-1}$, so, by Eq. (1), one finds the expression given in Eq. (3).

Appendix B: Relations between Fan Data and Expressions for Transillumination Geometry

Some geometrical corrections are required if we are to obtain from fan experimental data the corresponding transillumination contrast scan, $C_T(x, \Delta t)$.

First, in the framework of the random-walk model one can express the undistorted intensity $I_0^{(f)}(x, \Delta t)$ expected at the detector point x laterally shifted relative to the source as¹⁹

$$\begin{aligned} I_0^{(f)}(x, \Delta t) &= I_0^{(t)}(0, \Delta t) \frac{p_{\Delta t}(x)}{p_{\Delta t}(0)} \\ &= I_0^{(t)}(0, \Delta t) \exp(-3\mu_s' x^2 / 4c\Delta t), \end{aligned} \quad (\text{B1})$$

where $I_0^{(t)}(0, \Delta t)$ is the time-dependent intensity obtained in straight-through transmission (the distance between the detector and the source equals the distance across the slab) and where the ratio $p_{\Delta t}(x)/p_{\Delta t}(0)$ is derived from $p_n(x)/p_n(0) = \exp(-3x^2/4\Delta n)$ and $\Delta n = \mu_s' c\Delta t$.

Similarly, if x_0 is the position of the detector associated with the experimental, unperturbed path-

length distribution $I_0^{(f)}(x_0, \Delta t)$ taken as a reference, then the unperturbed path-length distribution to be expected at the detector shift x is determined by the ratio of corresponding probabilities:

$$\begin{aligned} I_0^{(f)}(x, \Delta t) &= I_0^{(f)}(x_0, \Delta t) \frac{p_{\Delta t}(x)}{p_{\Delta t}(x_0)} \\ &= I_0^{(f)}(x_0, \Delta t) \exp\left[-\frac{3\mu_s'(x^2 - x_0^2)}{4c\Delta t}\right]. \end{aligned} \quad (\text{B2})$$

Hence, using a derivation similar to that given in Ref. 15, one finds that, as a first approximation, in the fan geometry the distortion of the path lengths that is due to a small inclusion can be represented by the following expression:

$$\frac{\delta I^{(f)}(x, \Delta t)}{I_0^{(f)}(x, \Delta t)} = 1 - \frac{I^{(f)}(x, \Delta t)}{I_0^{(f)}(x, \Delta t)} = \eta_{\text{eff}} \frac{W^{(f)}(\mathbf{s}, \mathbf{x})_n}{p_n(x)}, \quad (\text{B3})$$

where η_{eff} is the effective absorptivity of the small inclusion considered. The corresponding intensity distortion expected in the case when the source is positioned over the target is

$$\begin{aligned} C_T(x, \Delta t) &= \frac{\delta I^{(t)}(x, \Delta t)}{I_0^{(t)}(\Delta t)} = \eta_{\text{eff}} \frac{W^{(t)}(\mathbf{s}, \mathbf{x})_{\Delta t}}{p_{\Delta t}(0)} \\ &= K_f \eta_{\text{eff}} \frac{W^{(f)}(\mathbf{s}, \mathbf{x})_n}{p_n(x)}, \end{aligned} \quad (\text{B4})$$

where

$$K_f = \frac{W^{(t)}(\mathbf{s}, \mathbf{x})_{\Delta t} p_{\Delta t}(x)}{W^{(f)}(\mathbf{s}, \mathbf{x})_{\Delta t} p_{\Delta t}(0)}. \quad (\text{B5})$$

Thus, from Eqs. (B2) and (B3) we finally have Eq. (10):

$$\begin{aligned} C_T(x, \Delta t) &= K_f \left[1 - \frac{I^{(f)}(x, \Delta t)}{I_0^{(f)}(x_0, \Delta t)} \frac{I_0^{(f)}(x_0, \Delta t)}{I_0^{(f)}(x, \Delta t)} \right] \\ &= \left[1 - \frac{I^{(f)}(x, \Delta t)}{I_0^{(f)}(x_0, \Delta t)} \frac{p_{\Delta t}(x_0)}{p_{\Delta t}(x)} \right] \\ &\quad \times \frac{W^{(t)}(\mathbf{s}, \mathbf{x})_{\Delta t} p_{\Delta t}(x)}{W^{(f)}(\mathbf{s}, \mathbf{x})_{\Delta t} p_{\Delta t}(0)}. \end{aligned} \quad (\text{B6})$$

The authors thank Simon Arridge for helpful discussions and for providing his inverse program for the calculation of its diffusion kernel.

References

1. B. Chance and R. R. Alfano, eds., *Optical Tomography, Photon Migration, and Spectroscopy of Tissue and Model Media: Theory, Human Studies, and Instrumentation*, Proc. SPIE **2389** (1995).
2. R. R. Alfano, ed., *Advances in Laser and Light Spectroscopy to Diagnose Cancer and Other Diseases*, Proc. SPIE **2387** (1995).
3. J. C. Hebden, S. R. Arridge, and D. T. Delpy, "Optical imaging in medicine. I. Experimental techniques," Phys. Biol. Med. **42**, 825–840 (1997).
4. S. R. Arridge and J. C. Hebden, "Optical imaging in medicine. II. Modelling and reconstruction," Phys. Biol. Med. **42**, 841–853 (1997).

5. T. L. Troy, D. L. Page, and E. M. Sevick-Muraca, "Optical properties of normal and diseased breast tissues: prognosis for optical tomography," *J. Biomed. Opt.* **1**, 342–355 (1996).
6. S. A. Walker, S. Fantini, and E. Gratton, "Image reconstruction by backprojection from frequency domain optical measurements in highly scattering media," *Appl. Opt.* **36**, 170–179 (1997).
7. H. B. Jiang, K. D. Paulsen, U. L. Osterberg, B. W. Pogue, and M. S. Patterson, "Optical image reconstruction using frequency domain data: simulations and experiments," *J. Opt. Soc. Am. A* **13**, 253–266 (1996).
8. M. A. O'Leary, D. A. Boas, and A. G. Yodh, "Experimental images of heterogeneous turbid media by frequency-domain diffusing photon tomography," *Opt. Lett.* **20**, 426–428 (1995).
9. J. C. Hebden, R. A. Kruger, and K. S. Wong, "Time-resolved imaging through a highly scattering medium," *Appl. Opt.* **30**, 788–794 (1991).
10. J. A. Moon and J. Reintjes, "Image resolution by use of multiply scattered light," *Opt. Lett.* **19**, 521–523 (1994).
11. A. H. Gandjbakhche, R. Nossal, and R. F. Bonner, "Resolution limits for optical transillumination of abnormalities embedded in tissues," *Med. Phys.* **22**, 185–191 (1994).
12. J. C. Hebden, D. J. Hall, and D. T. Delpy, "Time-resolved optical imaging of a solid tissue-equivalent phantom," *Med. Phys.* **22**, 201–208 (1995).
13. S. R. Arridge, "Photon measurement density functions: analytical forms," *Appl. Opt.* **34**, 7395–7409 (1995).
14. J. C. Hebden and S. R. Arridge, "Imaging through scattering media using an analytical model of perturbation amplitudes in the time-domain," *Appl. Opt.* **35**, 6788–6796 (1996).
15. A. H. Gandjbakhche, R. F. Bonner, R. Nossal, and G. H. Weiss, "Absorptivity contrast in transillumination imaging of tissue abnormalities," *Appl. Opt.* **35**, 1767–1774 (1996).
16. V. Chernomordik, R. Nossal, and A. H. Gandjbakhche, "Point spread functions of photons in time-resolved transillumination experiments using simple scaling argument," *Med. Phys.* **23**, 1857–1861 (1996).
17. A. H. Gandjbakhche and G. H. Weiss, "Random walk and diffusion-like model of photon migration in turbid media," in *Progress in Optics*, E. Wolf, ed. (Pergamon, London, 1995), Vol. 34, pp. 333–402.
18. A. H. Gandjbakhche, R. F. Bonner, and R. Nossal, "Scaling relationships for anisotropic random walks," *J. Stat. Phys.* **69**, 35–53 (1992).
19. A. H. Gandjbakhche, R. F. Bonner, R. Nossal, and G. H. Weiss, "Photon path-length distributions for transmission through optically turbid slabs," *Phys. Rev. E* **48**, 810–818 (1993).